Research Article | Vol. 29, No. 20 / 27 Sep 2021 / Optics Express 31632
Optics EXPRESS

Single-shot fringe pattern phase retrieval using improved period-guided bidimensional empirical mode decomposition and Hilbert transform

PAWEŁ GOCŁOWSKI,[1,3] MARIA CYWIŃSKA,[1] AZEEM AHMAD,[2] BALPREET AHLUWALIA,[2] AND MACIEJ TRUSIAK[1,4]

[1]Warsaw University of Technology, Institute of Micromechanics and Photonics, 8 Sw. A. Boboli St., 02-525 Warsaw, Poland
[2]Department of Physics and Technology, UiT The Arctic University of Norway, NO-9037 Tromsø, Norway
[3]pawel.goclowski@gmail.com
[4]maciej.trusiak@pw.edu.pl

Abstract: Fringe pattern analysis is the central aspect of numerous optical measurement methods, e.g., interferometry, fringe projection, digital holography, quantitative phase microscopy. Experimental fringe patterns always contain significant features originating from fluctuating environment, optical system and illumination quality, and the sample itself that severely affect analysis outcome. Before the stage of phase retrieval (information decoding) interferogram needs proper filtering, which minimizes the impact of mentioned issues. In this paper we propose fully automatic and adaptive fringe pattern pre-processing technique - improved period guided bidimensional empirical mode decomposition algorithm (iPGBEMD). It is based on our previous work about PGBEMD which eliminated the mode-mixing phenomenon and made the empirical mode decomposition fully adaptive. In present work we overcame key problems of original PGBEMD – we have considerably increased algorithm's application range and shortened computation time several-fold. We proposed three solutions to the problem of erroneous decomposition for very low fringe amplitude images, which limited original PGBEMD significantly and we have chosen the best one among them after comprehensive analysis. Several acceleration methods were also proposed and merged to ensure the best results. We combined our improved pre-processing algorithm with the Hilbert Spiral Transform to receive complete, consistent, and versatile fringe pattern analysis path. Quality and effectiveness evaluation, in comparison with selected reference methods, is provided using numerical simulations and experimental fringe data.

1. Introduction

The branch of optical full-field (non-scanning) fringe-based techniques, e.g., interferometry [1–3], digital holography [4,5], fringe projection [6] and moiré [7], plays an important role in various fields of modern science, such as biomedicine (non-invasive cell/tissue imaging) [8,9], 3D imaging [10], and experimental micromechanics (strain and stress evaluation) [11] etc. One of the main issues limiting the usefulness of fringe-based measurement methods is generally a cumbersome task of proper fringe patterns analysis [12]. Such analysis is based on solving the inverse problem and extracting the phase map from raw interferogram intensity distribution (phase map stores information about the measurand of interest). Optical full-field measurement is affected by several factors, like environment stability (temperature, air pressure, vibrations etc.) or optical system quality [1,2].

It is impossible to point out the best and the most universal method of fringe pattern analysis, mainly because there are two vital and usually exclusive measurement priorities: accuracy and speed. Temporal Phase Shifting (TPS) [1–2,13–14] techniques provide the best precision of

#435001 https://doi.org/10.1364/OE.435001
Journal © 2021 Received 24 Jun 2021; revised 14 Aug 2021; accepted 15 Aug 2021; published 17 Sep 2021

Optics EXPRESS

fringe pattern analysis; however, they belong to multi-frame analysis methods and thus require recording more than 3 fringe patterns, differed by the phase step. If TPS is planned to be used, optical system must be especially prepared, so that it can provide phase stepping. Multi-frame techniques enable relatively easy phase extraction and the highest accuracy for single-pixel resolution (phase values are calculated in each pixel separately) [1–2,13–14], but phase stepping elongates measurement time.

There are many applications, where measurement time is as crucial as its accuracy, e.g. time-lapse examination of rapidly moving biological objects or tomographic images [8]. Therefore single-frame fringe pattern analysis methods have been developed. Many of them are worth mentioning, for example: Fourier transform (FT) [15], windowed Fourier transform (WFT) [16], spatial carrier phase shifting (SCPS) [17], continuous wavelet transform (CWT) [18] and Hilbert spiral transform (HST) [19], to name some.

Single frame techniques enable quick and simple measurement, but they are more vulnerable to low signal to noise ratio (SNR) and varying fringe shapes (local period and orientation) [20]. In numerous scientific fields there is a strong desire of automatized fringe pattern analysis, but the mentioned difficulties make it an actual challenge, as optical data processing almost always needs some kind of human supervision. Among single-frame fringe pattern analysis techniques the Hilbert Spiral Transform (HST) [19] stands out as one of the most effective, versatile, and robust as it is an all-pass filter type of phase demodulation algorithm working without restrictions imposed on local shape of fringes – in contrary, e.g., to the FT, which needs high carrier frequency to ensure spectral separation of cross-correlation terms. The HST requires fringe pattern pre-processing, however. There are two crucial requirements, that must be fulfilled before performing successful HST: background inhomogeneity removal (i.e., to force fringe signal oscillation around zero mean value) and slowly-varying or non-existent amplitude modulation [19]. High noise level could also severely affect phase retrieval results (e.g., impending unwrapping of the phase map), making noise removal very desirable. Various pre-processing techniques fulfill these requirements, but come with a downside of long processing time and are highly parameter dependent (e.g., CWT [18] and Variational Image Decomposition (VID) [21]). Among them, recent improvements of Empirical Mode Decomposition (EMD) mark it out as unique and powerful approach.

Initially, EMD was proposed by Norden Huang in 1996 [22] as an adaptive and data driven method for nonlinear and nonstationary data analysis. Decomposition process is determined by the signal itself, basing on extrema distribution. Signal is decomposed into several intrinsic mode functions (IMF), representing consecutive, ascending inner scales of spatial frequencies. Development of bidimensional EMD (BEMD) [23,24] began an era of effectively applying this family of techniques into the fringe pattern analysis [25,26]. BEMD itself was an enormously time-consuming algorithm, however, as a consequence of using bidimensional cubic splines and radial based functions for interpolating envelope surfaces of the corresponding irregular 2D extrema maps. A significant improvement in computation time has been proposed by Bhuiyan et al. [27], replacing cubic splines with order-statistics-based filtering followed by a smoothing operation – algorithm is known as Fast Adaptive Bidimensional EMD (FABEMD). Further acceleration was provided by Trusiak et al. in Enhanced Fast EMD (EFEMD) algorithm [28]. Filtering window size was estimated using the number of extrema without resorting to costly calculation of the distance between adjacent extrema; envelope estimation as well as extrema detection was performed by means of the time-optimized morphological grayscale dilation.

The EFEMD algorithm and all its predecessors had a serious trouble due to the mode mixing phenomenon, understood as information spreading among several modes or mixing inside a single one [29]. In consequence, fringe information of various density was stored in several different modes. Fringe-containing modes had to be chosen manually, what impeded pre-processing automation and decreased its level of versatility and accuracy. In our previous work we proposed a solution to this important problem: Period Guided Bidimensional Mode Decomposition

Optics EXPRESS

(PGBEMD) algorithm [30]. We eliminated mode-mixing phenomenon, achieving crucial step in automation of the fully adaptive fringe pattern pre-processing. The working principle of PGBEMD relies on adaptive local filter size tailoring – we have applied small filter size in dense fringe areas and large filters in sparse fringe areas. Entire fringe information is now included in the first mode and background heterogeneity is removed. For more efficient noise removal, algorithm was also combined with block-matching 3D (BM3D) method [31]. It is important to note that PGBEMD alone works very well under noisy conditions, however incorporating the BM3D prevents the noise component to spoil the resulting phase distribution.

The PGBEMD, however, still suffers from certain issues and is not suitable for all kinds of interferograms. The first major issue, which restricts algorithm's versatility, refers to the low contrast images. Since numerous low-quality interferograms, exhibiting low fringe contrast and strong incoherent background illumination term, do not fulfill this condition, pushing the contrast limit is a crucial issue studied in this paper. Computation time stands out as the second major issue. Anti-mode-mixing improvements caused about fivefold elongation of the PGBEMD decomposition process compared to the EFEMD technique.

Thus, the main objective of this paper is to significantly improve the PGBEMD algorithm and overcome two main issues mentioned above, making it a truly versatile tool, capable of quick, automatic and adaptive pre-processing of any type of interferogram in a data-driven way. Proposed improved PGBEMD – the iPGBEMD algorithm, described in Section 2 – will be combined with phase demodulation performed by the HST creating comprehensive end-to-end fringe pattern analysis path, described in Section 3. Proposed method is numerically evaluated in Section 4 using various synthetic fringe patterns, along with reference methods: morphological operation based BEMD (MOBEMD) [32], unsupervised Variational Image Decomposition (uVID) [33] and original PGBEMD algorithm [30]. Last section of the paper provides experimental verification of image pre-processing and phase retrieval quality basing on real interferograms collected under laboratory conditions.

In all the following sections we will use Root Mean Square (RMS) error, received between calculated outcome and the numerical/experimental ground truth, to describe decomposition quality during quantitative evaluation. We use Matlab environment for all numerical analyses.

2. PGBEMD improvement: implementing the iPGBEMD

2.1. Pushing the fringe contrast limit

The EFEMD algorithm [28], PGBEMD predecessor, extracts the first mode function by subtracting the mean envelope from initial image. The next modes are extracted similarly, but the mean envelope from the previous iteration is treated as a new input image and filter size is bigger. In all iterations filter size is constant for the entire image, independently from local fringe density and as a result, fringe information of various density is stored in several different modes. In PGBEMD algorithm, mode-mixing has been avoided through spatially adaptive filter size introduction. This approach required local fringe density (fringe period) map estimation. Estimation we originally proposed in [30] works in a pixel-by-pixel manner on a single fringe pattern intensity distribution and contains the following steps:

1) Calculation of arithmetic average from the smallest pixel's neighborhood (3×3 pixels)
2) Calculation of local differences from this arithmetic average for every pixel in the neighborhood
3) Calculation of so-called Average Deviation (AvD, arithmetic average of those local differences)
4) Verification if AvD is larger than limit value, currently set as 50% of AvD calculated for the entire image: if this is true, neighborhood size is multiplied by 2 and saved as local

Optics EXPRESS

density, otherwise whole operation is repeated for consequently increasing neighborhoods (5×5, 7×7 etc.) until the condition is met

Local fringe period is used as a filter size for mode extraction in subsequent decomposition. The PGBEMD is sensitive to steep fringe slope, but in low-contrast images fringe slopes are not large enough compared to the background altitude, because AvD will not achieve the predefined limit value and will locally assign far too large density value to the pixels. It results in severe background leakage to the first mode and damage of the retrieved phase. To overcome this issue, we have proposed several improvements.

2.1.1. Search for the highest derivative of the Average Deviation parameter

We have investigated, how the AvD fluctuates in a function of the neighborhood size for three main cases: dense (Fig. 1(d)), moderately dense (Fig. 1(a)) and sparse fringes (Fig. 1(b)). For every case we calculated AvD for three adjoining pixels to prevent random errors.

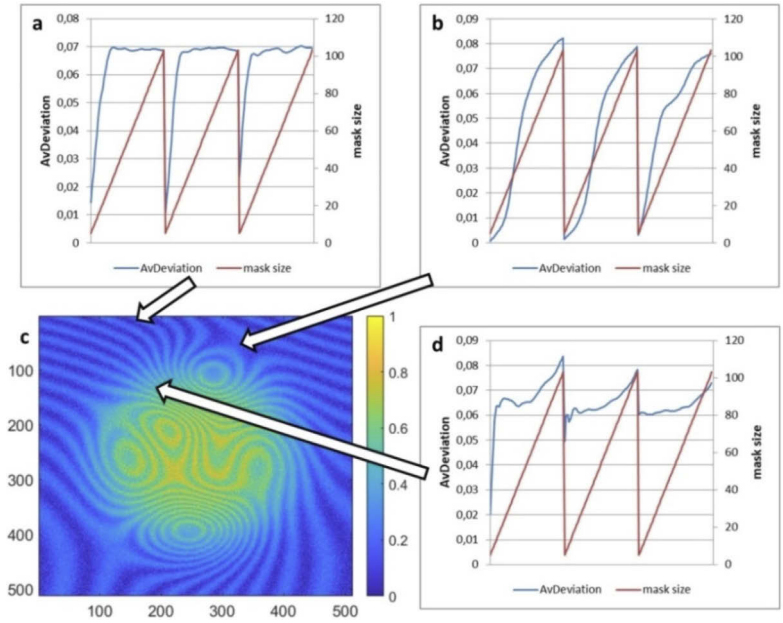

Fig. 1. AvD parameter in a function of the neighborhood size for moderately dense fringes (a), sparse fringes (b) and dense fringes (d) from exemplary simulated interferogram with low fringe contrast (c).

Figure 1 shows, that in dense fringe areas there occurs significant AvD function variation. It is less visible in sparse fringe case, but AvD parameter grows in differential rate, reaching highest growth in the middle of investigated range. Our first improvement idea is to change the stopping criterion for local density estimation. Filter size is now saved as local density when AvD derivative is the highest. This requires, however, calculation of AvD for entire range of mask sizes, making algorithm even more time-consuming.

2.1.2. Initial, coarse background estimation

As a second improvement concept to overcome erroneous decomposition for strong background-to-signal ratio we have decided to keep density calculation principle unchanged and reduce the background altitude initially in a fast and very versatile manner. Density map calculation is now preceded by initial, coarse background estimation, performed by image smoothing operation.

Optics EXPRESS

Value of every pixel is set as arithmetic average from its neighborhood. Initial smoothing uses a filter of very large size, currently set as quarter of image width, to ensure that no fringe information is lost at this stage. The simple filter we have created is an averaging, square-shaped one with adjustable size. It does not change its basic size, but if the pixel is near the edge of the image it becomes, for example, rectangular 9×7 or 9×5 instead of regular square 9×9. Algorithm does not search for pixel's neighborhood outside the image, so no data extrapolation is needed. It is similar to the one used in the decomposition process itself. As a result, low-frequency background distribution is received (Fig. 2(a)). Consequently, calculated distribution is subtracted from original image, significantly reducing the background altitude (Fig. 2(b)).

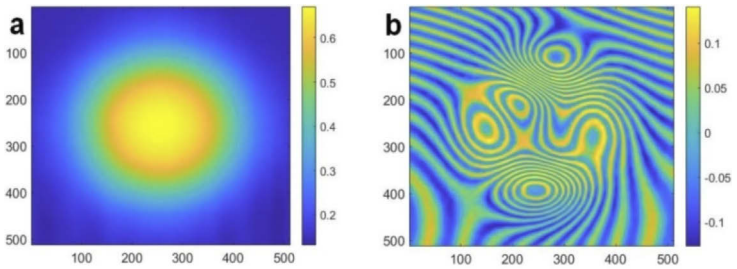

Fig. 2. Low spatial-frequency background distribution (a) estimated from the interferogram depicted in Fig. 1(c), and fringe pattern after subtraction of the coarse background (b).

2.1.3. Adaptive Average Deviation limit

Our third improvement idea is based on the preliminary determination of fringe contrast. The AvD limit is now made adaptive, in contrast to PGBEMD global one. It increases in the case of high fringe contrast and decreases in the case of low fringe contrast. For this purpose, initial, coarse background estimation is performed, same as in section 2.1.2. The difference is that background distribution is not subtracted from original image, we only acquire information about background altitude instead. Subsequently, we compare it with fringe altitude, acquired by subtracting background altitude from the range of input image intensity values. At the end AvD limit is multiplied by such estimated background-to-signal ratio. Scheme illustrating this procedure is shown on Fig. 3.

All simulated fringe patterns in this manuscript were in size of 512×512 pixels and were expressed with the following equation, unless otherwise stated:

$$image = contrast \cdot \cos(phase) + gauss + noise$$

where:

$$noise = abs(randn)$$

$$gauss = 10 \cdot normpdf(x^2 + y^2, 0, 3)$$

What is more, the phase of the exemplary interferogram from Figs. 1–3 is simulated as follows:

$$phase = x^{\frac{3}{5}} - 11 \cdot x - 2 \cdot y^2 + 10 \cdot y + 6 \cdot peaks$$

Effectiveness of all three improvements from sections 2.1.1–2.1.3 has been numerically compared in order to select the best solution. We investigated the RMS error between 1st mode from different variants of iPGBEMD and reference cosine of the simulated ground-truth phase – using the same exemplary interferogram, as in Figs. 1–3. Parameter c (fringe contrast defining the overall signal to background ratio of the fringe pattern) was established as a variable. Figure 4 shows RMS investigation results.

Optics EXPRESS

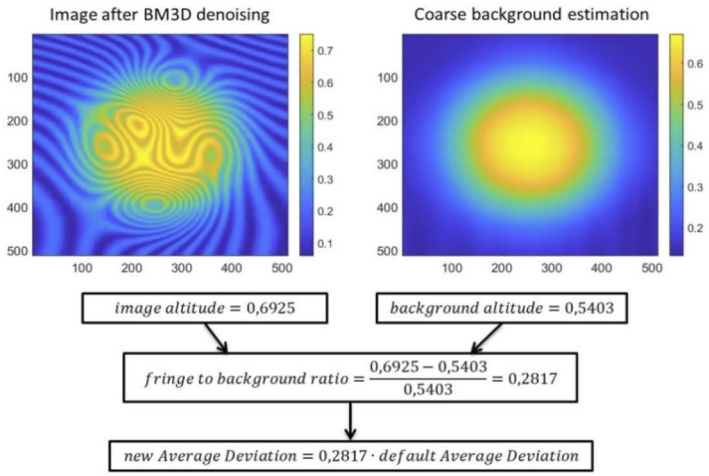

Fig. 3. Schematic illustration of adaptive AvD limit adjusting.

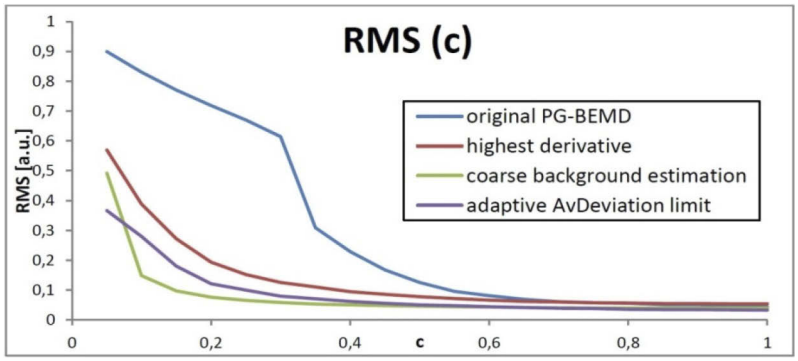

Fig. 4. RMS error of all proposed solutions in comparison to original PGBEMD decomposition comparison under varying fringe contrast.

Figure 4 clearly proves that all three proposed methods increased decomposition quality in low fringe contrast regime. Furthermore, we can undoubtedly state, that initial, coarse background estimation returns the best results. We have made an obvious decision to include that method in our enhanced iPGBEMD algorithm. Sufficient fringe contrast limit has been pushed down from 0.5 to around 0.2, considering competitive threshold of RMS=0.1. Decomposition of post-estimation image returns greatly improved 1st mode, see Fig. 5.

2.2. Accelerating the algorithm

The PGBEMD long computation time is a consequence of three main factors: BM3D denoising, local density map computation and the decomposition itself. Currently the PG-BEMD computation time varies between 20 and 40 seconds for 512×512 pixels images, processed on laptop with Intel Core i7-9750HF CPU and 16GB RAM (important note: all computation durations mentioned in this paper will refer to this computer). Relatively long processing time, although not precluding the preprocessing automatization, restricts algorithm's suitability for full-field interferometric data coming from regular CCD cameras (around 2000×3000 pixels). In this section we will concentrate on accelerating fringe density estimation, primarily. We propose three improvements accelerating the PGBEMD.

Optics EXPRESS

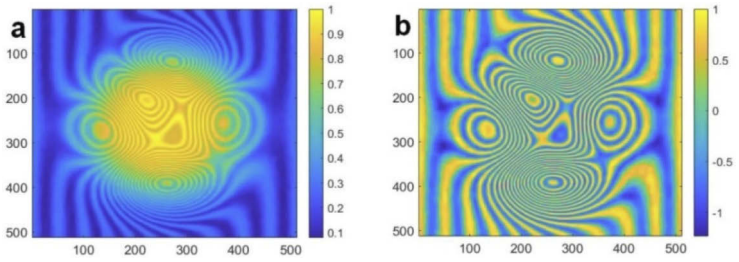

Fig. 5. The case of fringe contrast equal to 0.2: 1st mode extracted by original (a) and improved (b) PGBEMD.

2.2.1. Sparse sampling of the density map

While estimating the local fringe density, the PGBEMD repeatedly performs pixel-by-pixel operations and investigates large pixel neighborhoods. We have formed a hypothesis, that sparser sampling will have large impact on pre-processing time, while having a minor impact on the decomposition quality. We questioned our hypothesis, and calculated density of every third pixel in horizontal and vertical axis (every ninth, effectively) instead of doing it for every pixel. Density of remaining pixels were extrapolated from the nearest calculated one. Subsequently, we repeated experiment with density calculation of every fifth pixel, every seventh, every ninth etc. Decomposition quality and computation time have been evaluated in Fig. 6, depending on the fringe period map sampling rate.

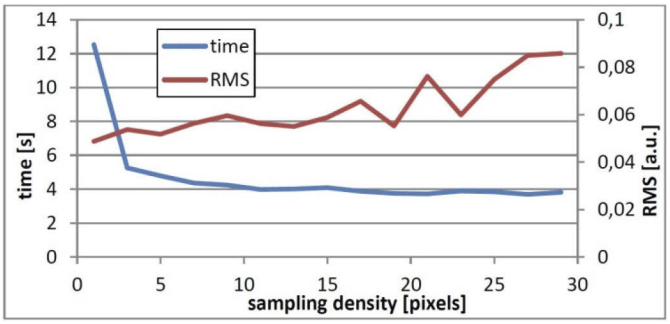

Fig. 6. RMS error and computation time depending on sampling density.

Outcomes presented in Fig. 6 prove, that small sampling rarefaction results in reasonably incremental RMS error increase, while it shortens the pre-processing duration significantly. Relationship between the RMS error, time and sampling density remains similar for many other simulated fringe patterns, therefore we decided to include only one such plot (derived for interferogram presented in Fig. 1(c)) in our paper. We chose sampling every fifth pixel for further analysis, but sampling rate remains parameterized and can be modified if needed.

2.2.2. Local density estimation guided by the adjacent values

Original PGBEMD algorithm always initiates density estimation from the smallest pixel's neighborhood (3×3) and increases neighborhood size until the AvD parameter reaches its predefined limit value. Therefore, investigation of all successive neighborhoods, especially in sparse fringe areas, is highly time consuming. In the novel iPGBEMD we propose the following modification: local density value from previous pixel serves as initial neighborhood size, and that

Optics EXPRESS

size can be either increased or decreased, depending on the AvD value. As a result, we managed to accelerate decomposition even more without any quality loss.

2.2.3. Removal of all further modes and merger of three acceleration concepts

After interferogram decomposition performed by PGBEMD entire fringe information is included in the first mode. Subsequent modes were still extracted, however, despite of providing non useful information. In iPGBEMD only the first mode is extracted, remaining mean envelope represents residual, background component.

Three proposed improvements combined allow to reduce the decomposition time greatly – about 6 times, from 30 to around 5 seconds for 512×512 images. We investigated decomposition process of two exemplary interferograms with the same phase function, but with different carrier spatial frequencies, verifying computation time for overall sparse and dense fringe patterns. Figures 7 and 8 show comparative charts between PGBEMD and iPGBEMD, respectively, pointing out fragmented computation time of every stage: BM3D denoising, density map calculation and decomposition.

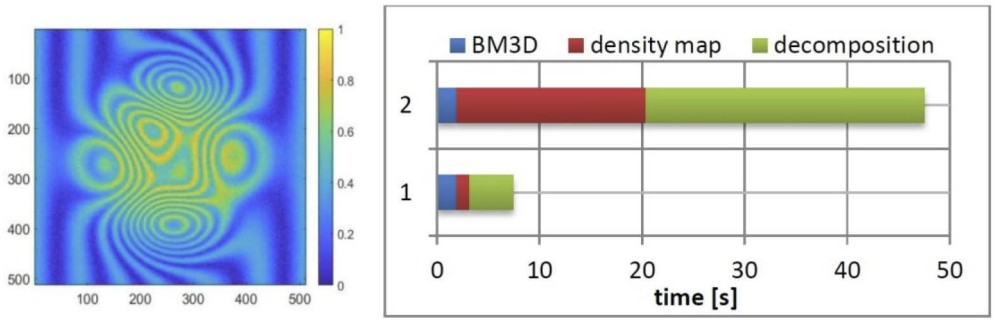

Fig. 7. Exemplifying input image (left) and the PGBEMD decomposition time before (2 - top right) and after (1 - bottom right) improvements.

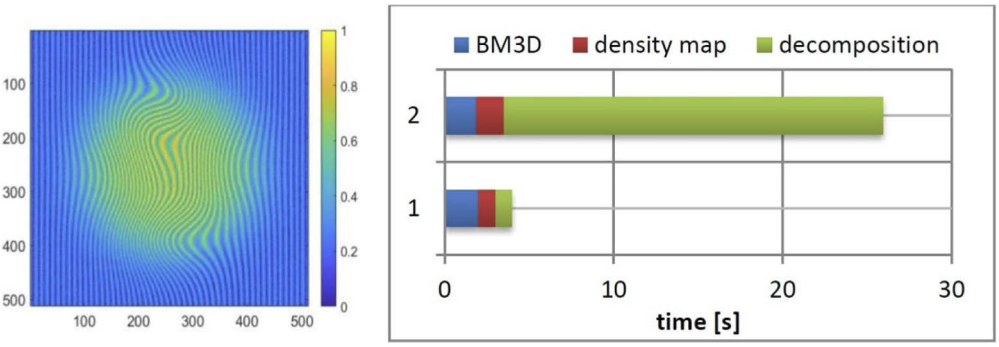

Fig. 8. Exemplifying input image (left) and the PGBEMD decomposition time before (2 - top right) and after (1 - bottom right) improvements.

The greatest advantage is achieved in duration of the decomposition itself, although for sparse fringe interferograms acceleration of density estimation becomes almost equally important. BM3D has not been accelerated and now it works through 25 to 50% of total pre-processing time. In case of low fringe pattern noise, it can be omitted thus reducing the pre-filtering time to around 2-5 seconds. Employing more sophisticated CPU hardware or implementing GPU

Optics EXPRESS

realization one could try to approach real time processing (8 frames per second). It is not the objective of this study, however, as we aim at low-cost and straightforward hardware.

3. Complete automatic interferogram analysis path

After improvements proposed in Sections 2.1 and 2.2 we have combined iPGBEMD with HST in order to create complete automatic interferogram analysis path. Main advantages of the HST in relation to other single-shot methods, which advocate the usage of HST for further analysis, are:

- easy automation – no special preparations in measurement technique and no manual window selection (like in Fourier Transform) are necessary;
- fully 2-D second frame generation;
- HST has already been successfully combined with previous empirical mode decomposition algorithms [22,25,28,34].

To sum up, we present all steps included in our novel analysis in a graphical way in Fig. 9. Processing path includes:

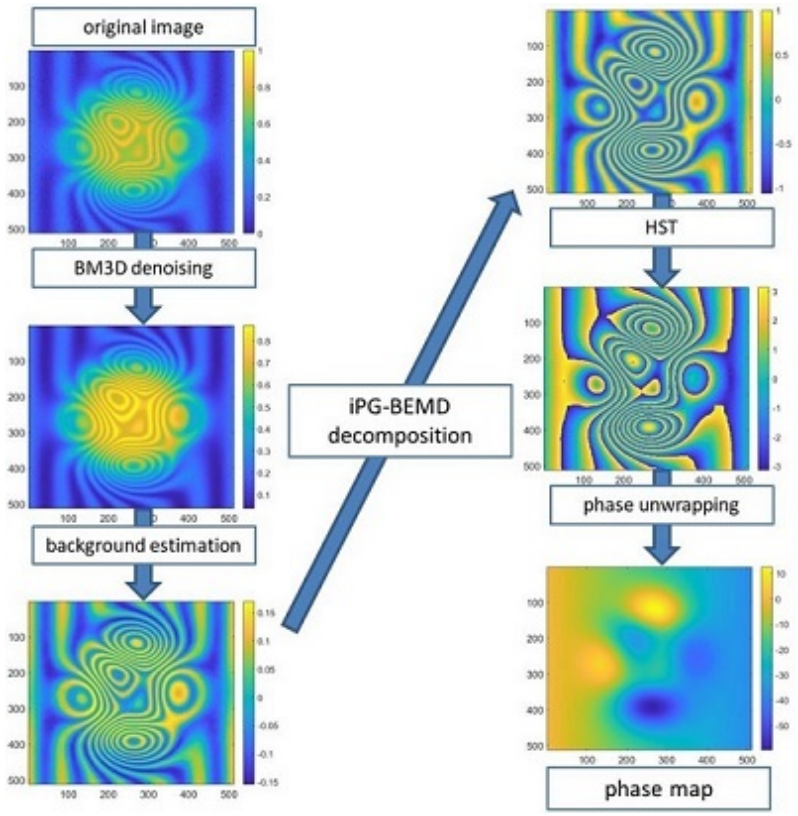

Fig. 9. Graphic scheme illustrating fringe pattern analysis using iPGBEMD + HST technique.

a) generation of synthetic interferogram in Matlab,

b) image denoising using BM3D algorithm – sigma parameter set to 60, wider analysis in our previous work [30],

Optics EXPRESS

c) initial background estimation performed by smoothing operation with very large (0.25 * M, where MxN is the image size), square-shaped, averaging filter,

d) subtracting the estimated background from the image,

e) density map calculation,

f) empirical mode decomposition, using local density value as local filter size, 1st mode extraction,

g) wrapped phase retrieval by Hilbert Spiral Transform,

h) phase unwrapping using Miguel 2D Unwrapper algorithm [35],

At the end we calculate the RMS error not only between 1st mode and ideal cosine of the phase, but also between retrieved phase and the reference simulated phase.

Since the visual difference, see Fig. 9, between the 1st mode and the image after coarse background estimation is relatively small, we have decided to compare decomposition results with hypothetical omission of that process – we have performed HST and phase unwrapping using image just after background estimation as input. The RMS error between calculated and ideal phase for original image from Fig. 9 is 0,2044 with iPGBEMD decomposition and 0,3972 without it (with simple coarse background removal only). Figure 10 presents error maps of both calculated phases. HST performs significantly worse without previous iPGBEMD decomposition – on Fig. 10(b) we can clearly see far larger errors than in Fig. 10(a).

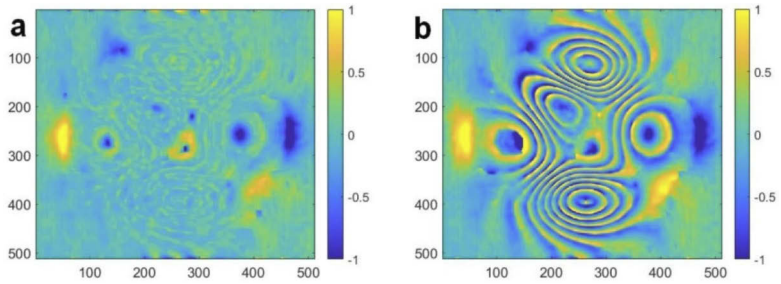

Fig. 10. Error map of retrieved phase with (a) and without (b) the iPGBEMD decomposition employment. In case of lack of iPGBEMD decomposition simple coarse background removal was implemented. The phase RMS dropped from around 0.4 to 0.2 radians after iPGBEMD incorporation.

4. Numerical evaluation using synthetic fringe patterns

Effectiveness of the presented technique has been numerically evaluated in broad and diverse tests. At first, we chose three reference pre-processing methods and compared, how they collaborate with HST.

The first chosen technique is the unsupervised Variational Image Decomposition (uVID), known for its good quality, but also for its long processing time. As the second method we chose Morphological Operation Based BEMD (MOBEMD), the reference technique in our previous work [30]. The last compared technique is original PGBEMD before improvements presented in this paper. We evaluated three main results for each method:

- RMS error between retrieved phase and reference phase,

- RMS error between fringe pattern after pre-processing and reference cosine of the phase,

Optics EXPRESS

- computation time.

Simulated fringe patterns were expressed with the following equations:

$$phase = a \cdot x + b \cdot peaks$$

$$Image = c \cdot \cos(phase) + gauss + d \cdot noise$$

We have investigated RMS and calculation time depending on the 5 factors, varying in a reasonable range:

- (1) carrier spatial frequency - parameter a - of linear fringes, see Fig. 11,
- (2) carrier spatial frequency - parameter a - of linear fringes with phase modulation, see Fig. 12,
- (3) dynamic range of the phase - parameter b, see Fig. 13,
- (4) fringe contrast - parameter c, see Fig. 14,
- (5) noise level - parameter d, see Fig. 15.

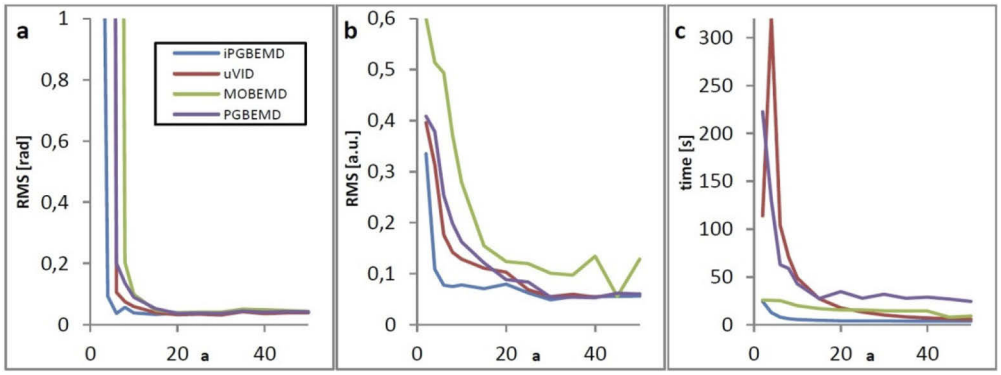

Fig. 11. RMS error of retrieved phase (a), RMS error after pre-processing (b) and computation time (c).

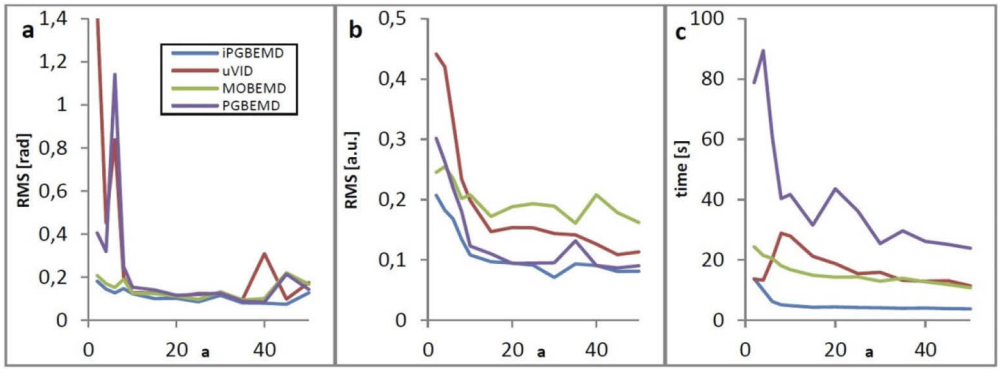

Fig. 12. RMS error of retrieved phase (a), RMS error after pre-processing (b) and computation time (c).

Optics EXPRESS

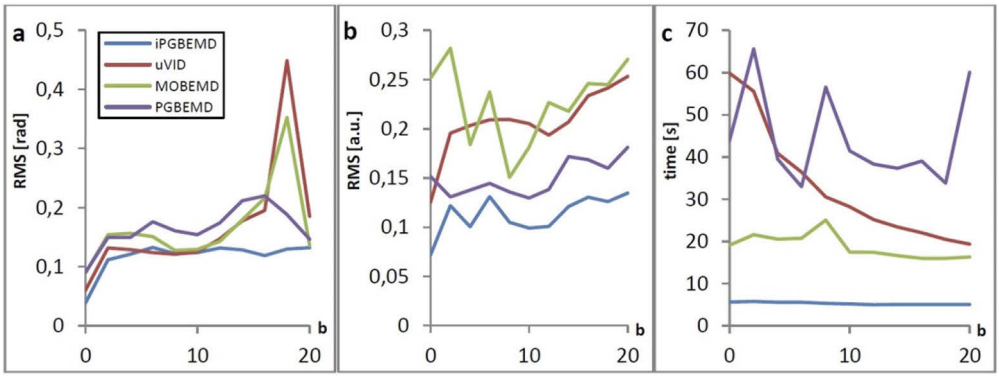

Fig. 13. RMS error of retrieved phase (a), RMS error after pre-processing (b) and computation time (c).

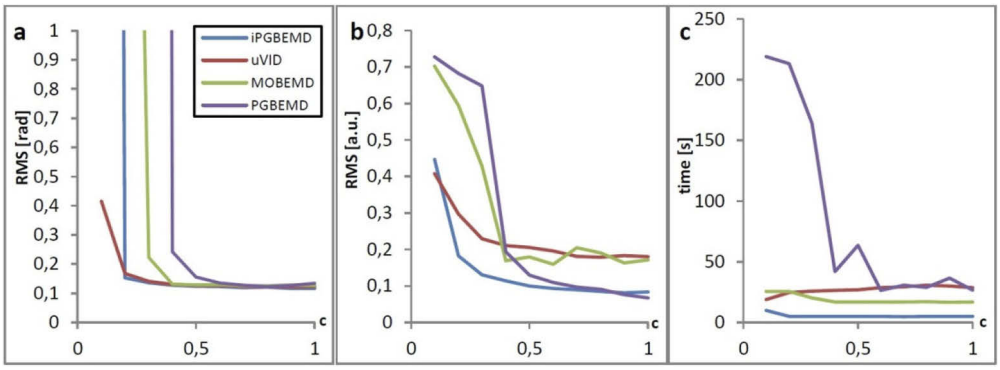

Fig. 14. RMS error of retrieved phase (a), RMS error after pre-processing (b) and computation time (c).

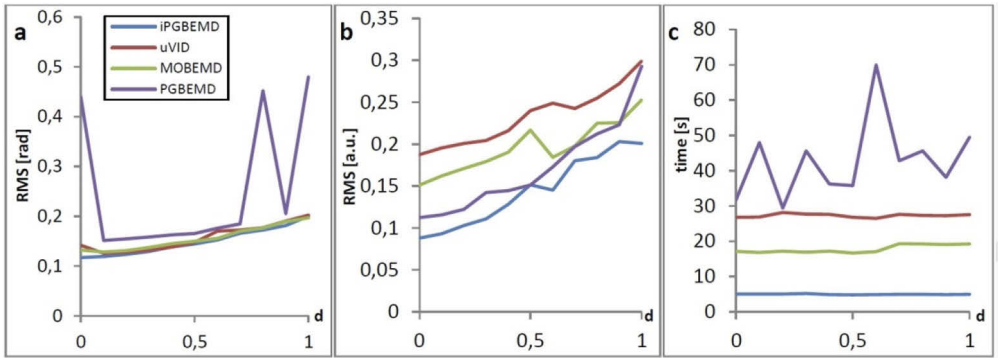

Fig. 15. RMS error of retrieved phase (a), RMS error after pre-processing (b) and computation time (c).

Optics EXPRESS

4.1. Variable carrier spatial frequency of linear fringes

Simulated fringe patterns were generated using the following formulae:

$$phase = a \cdot x$$

$$Image = 0.5 \cdot \cos(phase) + gauss + 0.2 \cdot noise$$

All fringe pattern pre-processing methods return lower RMS values for dense fringes rather than sparse fringes. There are, however, significant differences between them. The iPGBEMD achieves satisfactory quality already for a=5, while for other methods it is about 8-10. All techniques provide similar pre-processing and phase retrieval quality for dense linear fringes, however the MOBEMD is performing noticeably worse in case of pure pre-processing. It is worth mentioning, that the iPGBEMD provides the shortest computation time in the entire range of variable parameter a.

4.2. Variable carrier spatial frequency of closed fringes

Simulated fringe patterns were generated using the following formulae:

$$phase = a \cdot x + 10 \cdot peaks$$

$$Image = 0.5 \cdot \cos(phase) + gauss + 0.2 \cdot noise$$

Similarly, as in section 4.1 RMS error and computation time decrease with increasing carrier spatial frequency. The iPGBEMD outperforms all reference methods, especially in terms of quickness, achieving satisfactory overall time of 4-5 seconds.

4.3. Variable dynamic range of the phase

Simulated fringe patterns were generated using the following formulae:

$$phase = 10 \cdot x + b \cdot peaks$$

$$Image = 0.5 \cdot \cos(phase) + gauss + 0.2 \cdot noise$$

Larger dynamic range of the phase in most cases slightly increases RMS error of both phase retrieval and fringe pattern pre-processing. This effect is the least observable in the iPGBEMD, however. Our technique returns the most reliable and the fastest results. It is worth to notice that computation time of iPGBEMD is not only the shortest, but also the most stable and does not depend on the phase dynamic range (general variability of local optical path differences).

4.4. Variable fringe contrast

Simulated fringe patterns were generated using the following formulae:

$$phase = 10 \cdot x + 10 \cdot peaks$$

$$Image = c \cdot \cos(phase) + gauss + 0.2 \cdot noise$$

Figure 14 shows that none of the considered techniques deals properly with very low fringe contrast. There are, however, some important differences in their usefulness limit. The iPGBEMD and uVID are capable of properly decomposing images with fringe contrast larger than 0.2. For MOBEMD and original PGBEMD this is 0.3 and 0.4, respectively. Once again, the iPGBEMD proves itself to be the best and the fastest pre-processing tool among the tested representatives. It is also important to note how processing time is elongated for PGBEMD in low contrast regime, as algorithm is not able to converge.

Optics EXPRESS

4.5. Variable noise level

Simulated fringe patterns were generated using the following formulae:

$$phase = 10 \cdot x + 10 \cdot peaks$$

$$Image = 0.5 \cdot \cos(phase) + gauss + d \cdot noise$$

Presented plots show clearly that increasing noise level gradually increases the RMS error. The iPGBEMD achieves the best quality and the shortest calculation time for entire investigated range. It is worth mentioning, that all MOBEMD, uVID, PGBEMD and iPGBEMD methods include the same denoising technique – the BM3D.

5. Experimental validation

For the purpose of comprehensive iPGBEMD quality validation we take into account two experimental data sets – the first one was recorded during interferometric (Fizeau) evaluation of optical phase plate with varying shape of the front surface [36] and thus fringes encapsulate overall optical thickness variations (Fig. 16(a)). The second one represents HeLa(human cell line originating from cervical cancer) cells quantitative phase imaging (Fig. 17(a)). The first data set contained a total of 5 images, mutually phase shifted by $\pi/2$, but all compared techniques, excluding TPS, used only 1 out of 5 interferograms for further phase retrieval. HeLa cells were fixed and the temporal phase shifting was successfully captured in a Linnik type quantitative phase imaging interferometer [37–39].

In Figs. 16(a)-(j) we present pre-processing and phase retrieval results of the first experimental data set using 5 techniques: TPS, original PGBEMD + HST, iPGBEMD + HST, uVID + HST and MOBEMD + HST. All investigated techniques were generally competent, except for the MOBEMD where significant phase errors occurred on the upper edge (Fig. 16(j)). All the other phase maps exhibited hardly distinguishable differences, hence we decided to present phase error maps instead of very similar phase maps. Phase error map and consequent RMS error are calculated for each method as a difference between retrieved phase and the reference TPS phase map. Considering 1st modes extracted by PGBEMD (Fig. 16(b)), iPGBEMD (Fig. 16(e)), MOBEMD (Fig. 16(i)) and uVID texture component (Fig. 16(g)) we can state, that background removal in PGBEMD (RMS=0,3021) and iPGBEMD (RMS=0,3048) is better than in uVID (RMS=0,3587) and MOBEMD (RMS=0,3805), however comparing to uVID it has a very little impact on the final phase retrieval. It is worth to note, that original PGBEMD technique performs as good as the improved one – this is caused by relatively high fringe contrast in the input image.

Since obtaining ideal phase map from experimental data is practically impossible, in pursuit of better comparison we decided to treat the TPS-retrieved phase as the reference phase. We present the RMS error between TPS-retrieved phase and all the other phases in Table 1. We have also taken into account the computation time of the whole procedure, including HST and unwrapping. The RMS error is very similar for every method, except for MOBEMD, but iPGBEMD stands out as the indisputably fastest algorithm.

Table 1. Comparison of phase retrieval errors and computation time for phase plate examination.

Technique	RMS (in comparison to TPS)	Computation time [s]
PGBEMD	0,2142	108
iPGBEMD	0,2099	17
uVID	0,2076	132
MOBEMD	0,2493	52

Optics EXPRESS

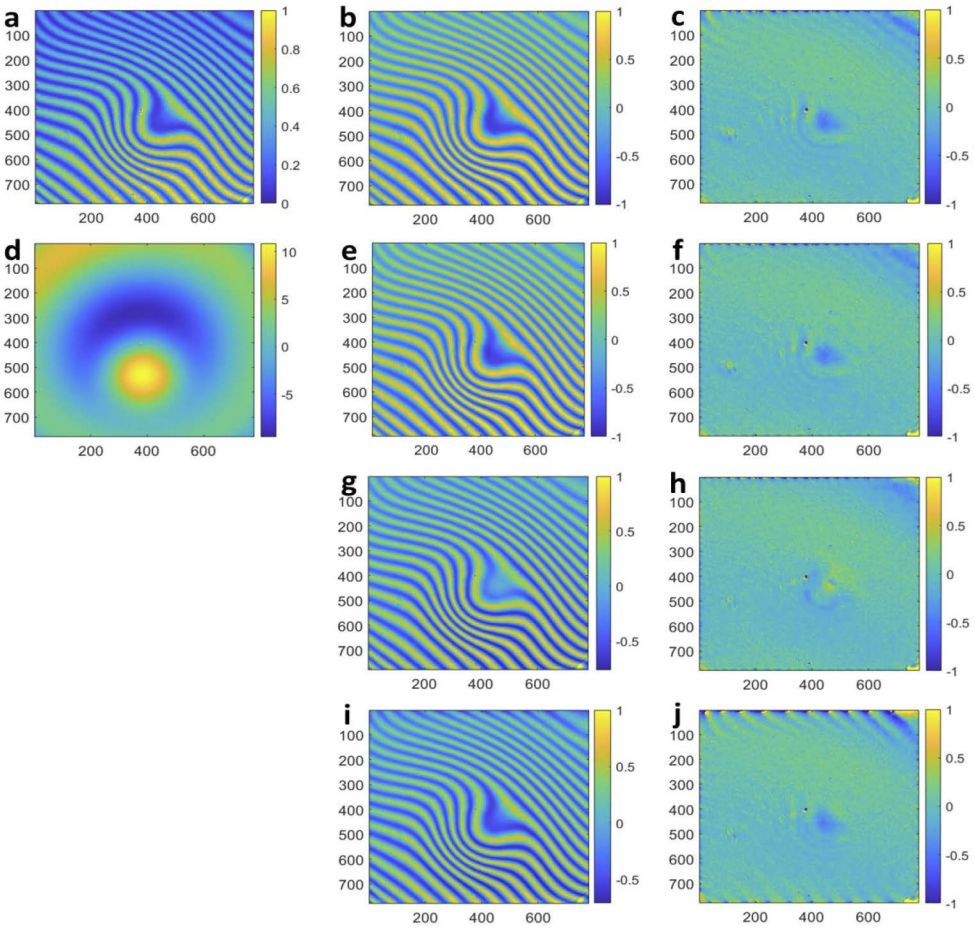

Fig. 16. Input image (a), 1st mode from original PGBEMD (b), original PGBEMD + HST error map (c), TPS-retrieved phase (d), 1st mode from iPGBEMD (e), iPGBEMD + HST error map (f), texture component from uVID (g), uVID + HST error map (h), 1st mode from MOBEMD (i) and MOBEMD + HST error map (j).

Optics EXPRESS

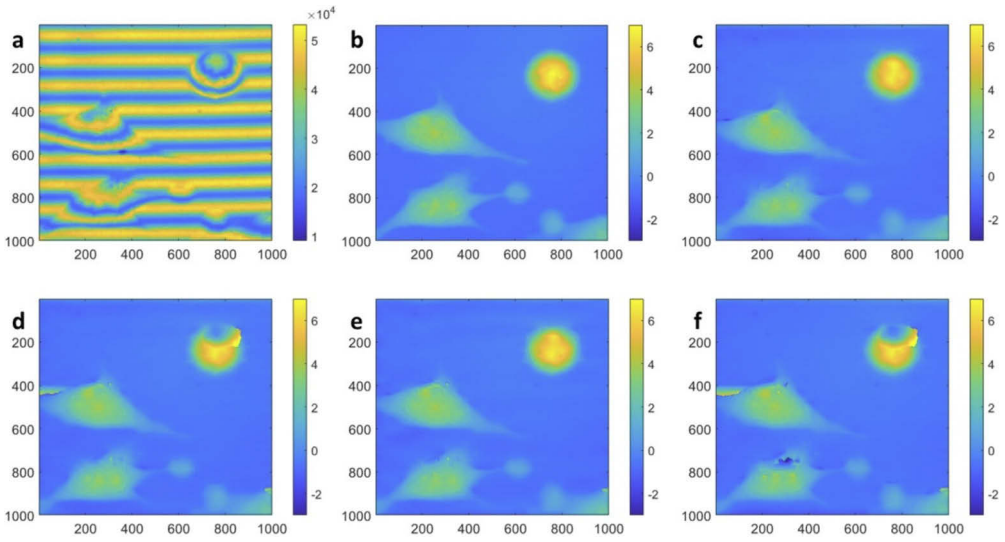

Fig. 17. HeLa cells: input image (a), TPS retrieved phase (b), iPGBEMD + HST retrieved phase (c), original PGBEMD + HST retrieved phase (d), MOBEMD + HST retrieved phase (e), and uVID + HST retrieved phase (f).

In Figs. 17 (c)-(g) we present the retrieved phase maps of the HeLa cells (Fig. 17(a)), using TPS, iPGBEMD, uVID, MOBEMD and original PGBEMD for fringe pattern pre-processing and HST for phase retrieval. The iPGBEMD (Fig. 17(c)) and MOBEMD (Fig. 17(e)) returned good results – cell shapes are correctly obtained, apart from minor punctual errors. The original PGBEMD results contain major discontinuities in two cells (Fig. 17(d)). The uVID performance was the most troublesome – significant errors are present in three cells (Fig. 17(f)).

Similar to experimental data from Fig. 16 we have decided to treat the TPS-retrieved phase as the reference phase. In Table 2 we present the RMS error between TPS-retrieved phase and all the other phase maps. Computation time of all methods is also presented. The iPGBEMD achieved the best RMS value, followed by MOBEMD, original PGBEMD, and uVID. The new iPGBEMD algorithm once again proves to be the fastest and the most efficient. Taking into account both experimental data sets its computation time is regularly 4 to 6 times shorter than in original PGBEMD. Processing time of all methods is significantly higher in comparison to numerical evaluation in section 4 due to larger image sizes (780×780 for Fig. 16(a) and 1000×1000 pixels for Fig. 17(a)).

Table 2. Comparison of phase retrieval errors and computation time for HeLa cells examination.

Technique	RMS (in comparison to TPS)	Computation time [s]
PGBEMD	0,4325	211
iPGBEMD	0,1772	45
uVID	0,4986	679
MOBEMD	0,1829	90

Optics EXPRESS

6. Conclusions

Fringe pattern enhancement and phase retrieval automatization are highly desirable features in many contemporary optical measurements. To fulfill this important need and fill the state-of-the-art gap we proposed an adaptive, versatile and efficient interferogram analysis path using improved Period Guided Bidimensional Empirical Mode Decomposition and Hilbert Spiral Transform. We have reduced computation time greatly by merging sparse sampling rate, density map optimization using adjacent density values and removal of further modes extraction. Due to simple, but effective idea of initial coarse background estimation and subtraction we have managed to deal with the most important problem of original PGBEMD: bad immunity to low fringe contrast. The novel iPGBEMD is later combined with the Hilbert Spiral Transform, and as a result both techniques cooperate perfectly with each other. We tested out how broad range of factors affect decomposition, including fringe carrier spatial frequency, dynamic range of the phase, fringe contrast and noise levels. Wide numerical evaluation proved iPGBEMD to be superior to every reference method, including unsupervised Variational Image Decomposition (uVID), Morphological Operation Based Empirical Mode Decomposition (MOBEMD) and original PGBEMD. Experimental validation, executed upon phase plate interferometric analysis and HeLa cells quantitative phase imaging, corroborated unique capabilities (short time, high accuracy and versatility) of the novel single shot phase demodulation approach. Our algorithm has also provided the shortest computation time among all reference methods in both numerical and experimental validation. Proposed iPGBEMD technique is undoubtedly suitable for a wide range of applications for efficient and automatic fringe pattern enhancement in numerous fields of contemporary science and technology, e.g. biomedicine, 3D imaging and experimental micromechanics.

The iPGBEMD algorithm has been implemented as we show in Code 1, Ref. [40].

Funding. Politechnika Warszawska (ID-UB: FOTECH-1); Narodowe Centrum Nauki (2020/37/B/ST7/03629).

Acknowledgments. This work has been supported by the Warsaw University of Technology statutory funds. Authors thank PhD Zofia Sunderland for providing access to interferograms of optical plate (Fig. 16).

Disclosures. The authors declare no conflicts of interests.

Data availability. Data underlying the results presented in this paper are not publicly available at this time but will be made available upon reasonable request.

References

1. D. Malacara ed., *Optical Shop Testing* (Jon Wiley and Sons, 2007).
2. M. Servin, J. A. Quiroga, and M. Padilla, Fringe Pattern Analysis for Optical Metrology: Theory, *Algorithms, and Applications* (Wiley, 2014).
3. D. W. Robinson and G. Reid, *Interferogram Analysis: Digital Fringe Pattern Measurement* (Institute of Physics Publishing, 1993).
4. U. Schnars and W.P. Jueptner, *Digital Holography* (Springer, 2005).
5. L.P. Yaroslavsky, Digital Holography and Digital Image Processing: Principles, Methods, *Algorithms* (Kluwer, 2003).
6. W. Schreiber and G. Notni, "Theory and arrangements of self-calibrating whole-body 3-D-measurement systems using fringe projection technique," Opt. Eng. **39**(1), 159 (2000).
7. K. Patorski and M. Kujawinska, *Handbook of the moiré fringe technique* (Elsevier Science Limited, 1993).
8. Y. Park, C. Depeursinge, and G. Popescu, "Quantitative phase imaging in biomedicine," Nat. Photon **12**(10), 578–589 (2018).
9. N.T. Shaked, Y. Zhu, M.T. Rinehart, and A. Wax, "Two-step-only phase-shifting interferometry with optimized detector bandwidth for microscopy of live cells," Opt. Express **17**(18), 15585–15591 (2009).
10. Jason Geng, "Structured-light 3D surface imaging: a tutorial," Adv. Opt. Photon. **3**(2), 128–160 (2011).
11. V. Pisarev, I. Odintsev, S. Eleonsky, and A. Apalkov, "Residual stress determination by optical interferometric measurements of hole diameter increments," Opt. Lasers Eng. **110**, 437–456 (2018).
12. G.T. Reid, "Automatic fringe pattern analysis: A review," Opt. Lasers Eng. **7**(1), 37–68 (1986).
13. K. Creath, *Temporal phase measurement methods* (Institute of Physics Publishing, 1993).
14. J. Schwider, "Advanced evaluation techniques in interferometry," Prog. Opt. **28**, 271–359 (1990).
15. M. Takeda, H. Ina, and S. Kobayashi, "Fourier-transform method of fringe-pattern analysis for computer-based topography and interferometry," J. Opt. Soc. Am. **72**(1), 156–160 (1982).

Optics EXPRESS

16. Q. Kemao, "Windowed Fourier transform for fringe pattern analysis," Appl. Opt. **43**(13), 2695–2702 (2004).
17. M. Kujawinska and J. Wojciak, "Spatial-carrier phase-shifting technique of fringe pattern analysis," Proc. SPIE **1508**, 61–67 (1991).
18. Z. Wang and H. Ma, "Advanced continuous wavelet transform algorithm for digital interferogram analysis and processing," Opt. Eng. **45**(4), 045691 (2006).
19. K. G. Larkin, D. J. Bone, and M. A. Oldfield, "Natural demodulation of two-dimensional fringe patterns. I. General background of the spiral phase quadrature transform," J. Opt. Soc. Am. A **18**(8), 1862–1870 (2001).
20. J.J. Talamonti, R.B. Kay, and D.J. Krebs, "Numerical model estimating the capabilities and limitations of the fast Fourier transform technique in absolute interferometry," Appl. Opt. **35**(13), 2182–2191 (1996).
21. X. Zhu, Z. Chen, and C. Tang, "Variational image decomposition for automatic background and noise removal of fringe patterns," Opt. Lett. **38**(3), 275–277 (2013).
22. N. E. Huang, Z. Shen, S. R. Long, M. C. Wu, H. H. Shih, Q. Zheng, N.-C. Yen, C. C. Tung, and H. H. Liu, "The empirical mode decomposition and the Hilbert spectrum for non-linear and non-stationary time series analysis," Proc. R. Soc. Lond. A **454**(1971), 903–995 (1998).
23. C. Damerval, S. Meignen, and V. Perrier, "A fast algorithm for bidimensional EMD," IEEE Signal Process. Lett. **12**(10), 701–704 (2005).
24. J. C. Nunes, Y. Bouaoune, E. Delechelle, O. Niang, and Ph. Bunel, "Image analysis by bidimensional empirical mode decomposition," Image Vis. Comput. **21**(12), 1019–1026 (2003).
25. M.B. Bernini, A. Federico, and G.H. Kaufmann, "Normalization of fringe patterns using the bidimensional empirical mode decomposition and the Hilbert transform," Appl. Opt. **48**(36), 6862–6869 (2009).
26. M.B. Bernini, A. Federico, and G.H. Kaufmann, "Noise reduction in digital speckle pattern interferometry using bidimensional empirical mode decomposition," Appl. Opt. **47**(14), 2592–2598 (2008).
27. S. M. A. Bhuiyan, R. R. Adhami, and J. F. Khan, "Fast and adaptive bidimensional empirical mode decomposition using order-statistics filter based envelope estimation," EURASIP J. Adv. Signal Process. **2008**(164), 725356 (2008).
28. M. Trusiak, M. Wielgus, and K. Patorski, "Advanced processing of optical fringe patterns by automated selective reconstruction and enhanced fast empirical mode decomposition," Opt. Lasers Eng. **52**(1), 230–240 (2014).
29. Y. Yang, J. Deng, and C. Wu, "Analysis of Mode Mixing Phenomenon in the Empirical Mode Decomposition Method," *Second International Symposium on Information Science and Engineering*, 553–556 (2009).
30. P. Gocłowski, M. Trusiak, A. Ahmad, A. Styk, V. Mico, B. S. Ahluwalia, and K. Patorski, "Automatic fringe pattern enhancement using truly adaptive period-guided bidimensional empirical mode decomposition," Opt. Express **28**(5), 6277–6293 (2020).
31. K. Dabov, A. Foi, V. Katkovnik, and K. Egiazarian, "Image denoising by sparse 3-D transform-domain collaborative filtering," IEEE Trans. Image Process. **16**(8), 2080–2095 (2007).
32. X. Zhou, A. Gh. Podoleanu, Z. Yang, T. Yang, and H. Zhao, "Morphological operation-based bi-dimensional empirical mode decomposition for automatic background removal of fringe patterns," Opt. Express **20**(22), 24247–24262 (2012).
33. M. Cywinska, M. Trusiak, and K. Patorski, "Automatized fringe pattern preprocessing using unsupervised variational image decomposition," Opt. Express **27**(16), 22542–22562 (2019).
34. M. Wielgus and K. Patorski, "Evaluation of amplitude encoded fringe patterns using the bidimensional empirical mode decomposition and the 2D Hilbert transform generalizations," Appl. Opt. **50**(28), 5513–5523 (2011).
35. M. A. Herráez, D. R. Burton, M. J. Lalor, and M. A. Gdeisat, "Fast two-dimensional phase-unwrapping algorithm based on sorting by reliability following a noncontinuous path," Appl. Opt. **41**(35), 7437–7444 (2002).
36. Z. Sunderland, K. Patorski, and M. Trusiak, "Subtractive two-frame three-beam phase-stepping interferometry for testing surface shape of quasi-parallel plates," Opt. Express **24**(26), 30505–30513 (2016).
37. A. Butola, S.R. Kanade, S. Bhatt, V.K. Dubey, A. Kumar, A. Ahmad, D.K. Prasad, P. Senthilkumaran, B.S. Ahluwalia, and D.S. Mehta, "High space-bandwidth in quantitative phase imaging using partially spatially coherent digital holographic microscopy and a deep neural network," Opt. Express **28**(24), 36229–36244 (2020).
38. V. Dubey, D. Popova, A. Ahmad, G. Acharya, P. Basnet, D.S. Mehta, and B.S. Ahluwalia, "Partially spatially coherent digital holographic microscopy and machine learning for quantitative analysis of human spermatozoa under oxidative stress condition," Sci. Rep. **9**(1), 3564 (2019).
39. A. Butola, D. Popova, D.K. Prasad, A. Ahmad, A. Habib, J.C. Tinguely, P. Basnet, G. Acharya, P. Senthilkumaran, D.S. Mehta, and B.S. Ahluwalia, "High spatially sensitive quantitative phase imaging assisted with deep neural network for classification of human spermatozoa under stressed condition," Sci. Rep. **10**(1), 13118 (2020).
40. P. Goclowski and M. Trusiak, "Single-shot fringe pattern phase retrieval using improved period-guided bidimensional empirical mode decomposition and Hilbert transform: supporting code," GitHub (2021) [accessed 17 August 2021], https://github.com/Delorro/iPG-BEMD.